

# Simulation Analysis of Dust-Particle Transport in the Peripheral Plasma in the Large Helical Device<sup>\*)</sup>

Mamoru SHOJI, Yasunori TANAKA<sup>1)</sup>, Alexander Yu. PIGAROV<sup>2)</sup>, Roman D. SMIRNOV<sup>2)</sup>,  
Suguru MASUZAKI, Gakushi KAWAMURA, Yoshihiko UESUGI<sup>1)</sup>, Hiroshi YAMADA  
and the LHD Experiment Group

*National Institute for Fusion Science, 322-6 Oroshi-cho, Toki 509-5292, Japan*

<sup>1)</sup>*Kanazawa University, Kakuma, Kanazawa 920-1192, Japan*

<sup>2)</sup>*University of California at San Diego, La Jolla, CA 92093, USA*

(Received 18 November 2013 / Accepted 9 July 2014)

The function of the peripheral plasma in the Large Helical Device (LHD) on transport of dusts is investigated using a dust transport simulation code (DUSTT) in a non-axisymmetric geometry. The simulation shows that the transport of the dusts is dominated by the plasma flow (mainly by ion drag force) formed in the peripheral plasma. The trajectories of dusts are investigated in two probable situations: release of spherical iron dusts from the inboard side of the torus, and drop of spherical carbon dusts from a divertor plate installed near an edge of an upper port. The trajectories in these two situations are calculated in various sized dust cases. From a viewpoint of protection of the main plasma from dust penetration, it proves that there are two functions in the LHD peripheral plasma. One is sweeping of dusts by the effect of the plasma flow in the divertor legs, and another one is evaporation/sublimation of dusts by heat load onto the dusts in the ergodic layer.

© 2014 The Japan Society of Plasma Science and Nuclear Fusion Research

Keywords: dust transport simulation, DUSTT, peripheral plasma, divertor, LHD

DOI: 10.1585/pfr.9.3403132

## 1. Introduction

The transport of dusts in magnetic plasma confinement devices has been attracting attention because it can affect plasma performances. Termination of ICRF heated long pulse discharges in the Large Helical Device (LHD), which synchronized with so called ‘spark’ events in the vacuum vessel, was observed, resulting in injection of iron into the main plasma [1]. High- $\beta$  plasmas have often been interrupted by core density collapse (CDC) by drop of a large amount of dusts induced by intense plasma-wall interactions caused by abrupt particle exhaust from the main plasma [2], and the characteristics of dusts in (morphology, size distributions and the composition) was also investigated in LHD [3, 4]. In this paper, the trajectories of dusts calculated by a dust transport simulation code in a non-axisymmetric geometry are presented. The calculations of the time evolution of dust parameters (the temperature, mass and velocity) for various sized dusts are also shown.

## 2. Setup for Dust Transport Simulation

A dust transport simulation code (DUSTT) has been developed for investigating the effect of dusts on peripheral

plasmas in axisymmetric plasma confinement devices such as Tokamaks [5–7]. This code can calculate the time evolution of the force, heat, energy and charge balances in spherical dusts in plasmas. It can treat dusts composed of almost all elements possibly used in the vacuum vessels. There is a problem to apply the code to non-axisymmetric geometries such as LHD because the code is strongly coupled with a two-dimensional plasma fluid code (UEDGE) [8]. To solve this, a sub-program for tracking the dust trajectories in the DUSTT was modularized and implemented into a neutral particle transport simulation code (EIRENE) [9]. In this modified EIRENE, dusts are treated as virtual neutral particles having a statistical weight representing the dust size (radius). Profiles of background plasma parameters (ion/electron density and temperature, plasma flow velocities, etc.) are supplied from a three-dimensional edge plasma fluid code (EMC3) coupled with the EIRENE in a standard magnetic configuration (the radial position of the magnetic axis:  $R_{ax} = 3.60$  m) [10]. In the calculation by the EMC3-EIRENE code, the heating power and the plasma density at the Last Closed Flux Surface (LCFS) have to be fixed as initial conditions.

Figure 1 shows bird’s-eye view of a model of the LHD three-dimensional geometry with the calculated plasma flow velocity distribution along the magnetic field lines in the case where the heating power and the plasma density at the LCFS ( $P^{LCFS}$  and  $n_c^{LCFS}$ ) are 2 MW and  $2 \times 10^{19} \text{ m}^{-3}$ ,

author’s e-mail: shoji@LHD.nifs.ac.jp

<sup>\*)</sup> This article is based on the presentation at the 23rd International Toki Conference (ITC23).

respectively. These two parameters are chosen for investigating the effect of dusts in ICRF heated long pulse discharges targeted in the near future. Thus, the simulations will be a guide line for optimizing the operational regime for the long pulse discharges. The LHD peripheral plasma consists of two magnetic structures: an ergodic layer and divertor legs. The typical plasma temperature in the divertor legs and that at the outer edge of the ergodic layer, which are calculated by the EMC3-EIRENE, are about 20 eV and 50 eV, respectively.

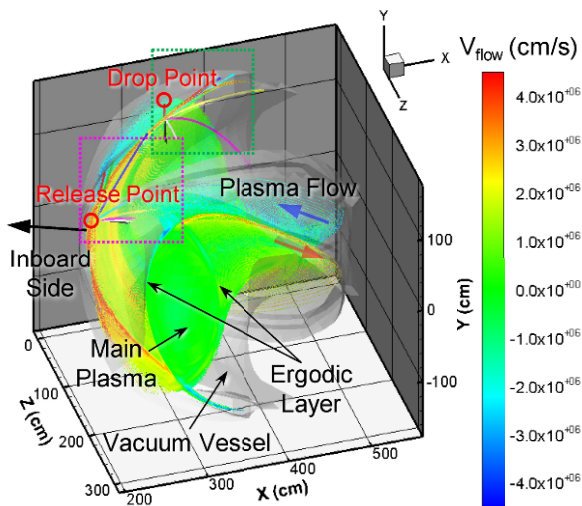


Fig. 1 Bird's-eye view of the three-dimensional LHD geometry with the calculated plasma flow velocity distribution (shown as small colored dots). The positive sign of the plasma flow means that the direction of the flow is toroidally counterclockwise when it is viewed from the upper side (+Y axis side).

### 3. Dust Transport Analysis using the DUSTT

In order to investigate the effect of the LHD peripheral plasma on transport of dusts, the following two probable situations are considered:

1. Release of spherical iron dusts from a divertor plate installed in the inboard side of the torus,
2. Drop of spherical carbon dusts from a vertically installed divertor plate near an edge of an upper port.

The reason for investigating the first situation is that ICRF heated long pulse discharges were terminated by release of dusts with sparks near the inboard side of the torus in the 2004y experimental campaign in which the drastic increase of the emission by iron ions synchronized with plasma termination was observed. In the standard magnetic configuration, most of the particle/heat flux from the main plasma is localized to the inboard side. It is possible that dusts consisting of sputtered materials from the vacuum vessel (mainly iron), which have been accumulated on divertor plates, are exfoliated and released by interactions with the peripheral plasma on the divertor plates. For the second situation, a tangentially viewing fast framing camera observed that a few dusts dropped from a position just under a vertically installed divertor plate in a recent ICRF heated long pulse discharge. The divertor plate could be locally heated by fast ions accelerated by ICRF waves near the antennas, leading to the drop of dusts consisting of the element of the divertor plate (carbon) induced by thermal distortion on the surface of the divertor plate.

The dust trajectories are calculated for various initial dust radii ( $r_{dust}$ ) which are in the range of the dusts collected in the vacuum vessel after experimental campaigns (except for  $r_{dust} = 1$  mm) [11]. In the simulation, the particle reflection coefficient of dusts on the vacuum vessel and

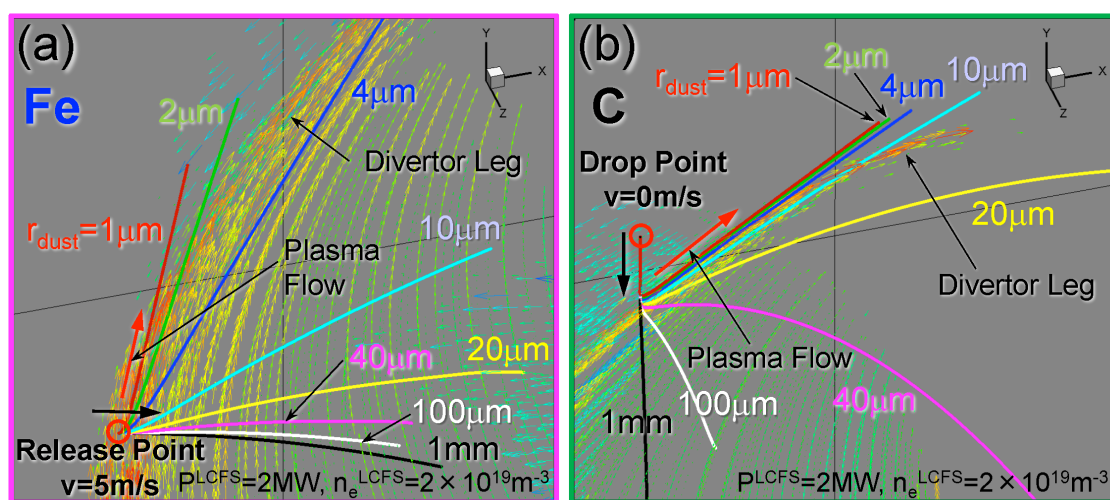


Fig. 2 Calculated trajectories of spherical iron dusts released from the inboard side of the torus for the first situation (a), and those of carbon dusts dropped from the upper side in the second situation (b). The initial positions of the dusts are indicated as open red circles. Colored lines represent the trajectories for various dust radii. The direction of the plasma flow on the peripheral plasma is indicated as small colored vectors. The positions of the frames of these two figures correspond to broken purple and green squares in Fig. 1, respectively.

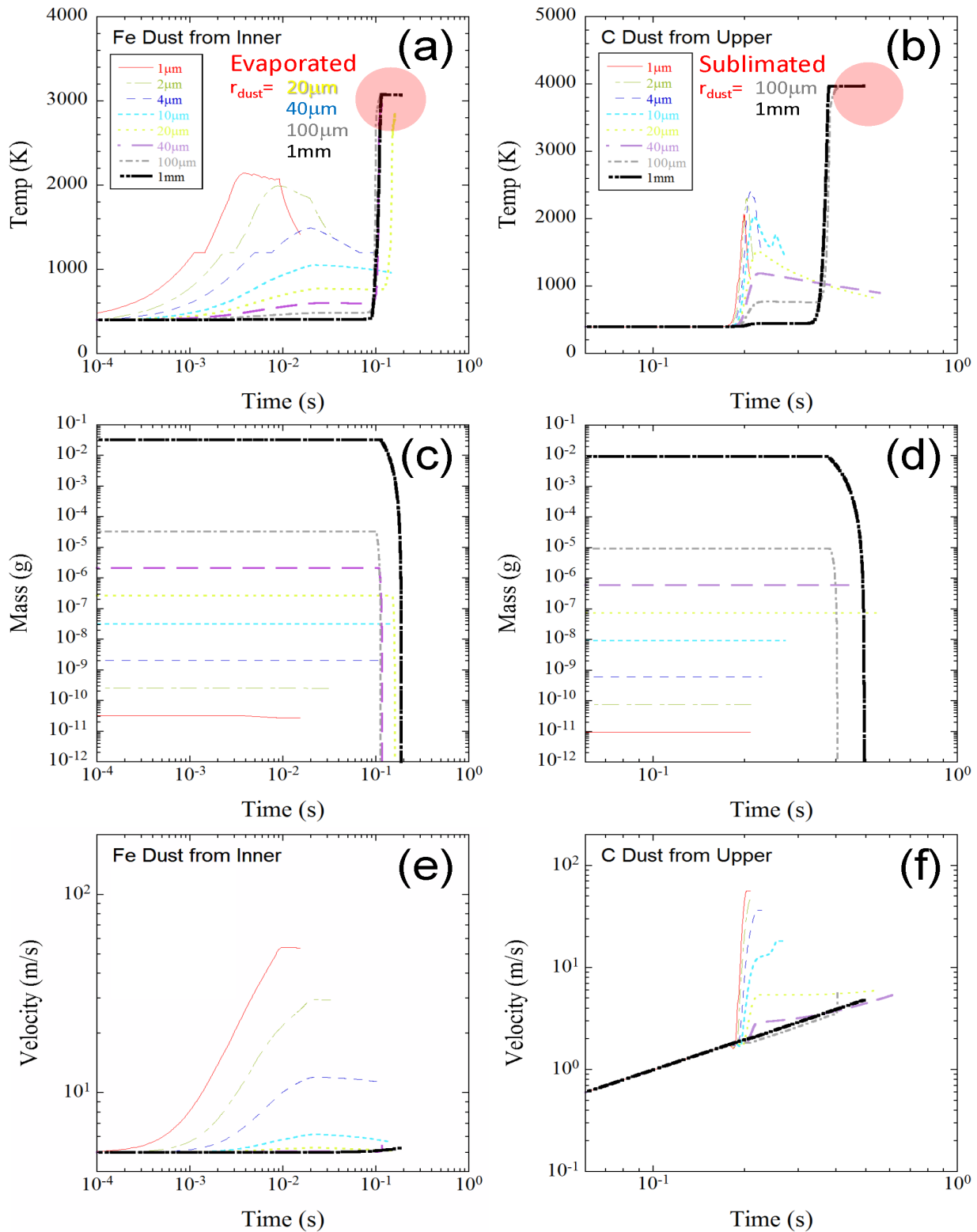


Fig. 3 Time evolutions of the dust temperature (a, b), mass (c, d) and velocity (e, f) calculated by the DUSTT code implemented in the EIRENE for various initial dust radii. Graphs in the left and right column are the time trends of the dust parameters for the first (iron dusts) and second (carbon dusts) situations, respectively. Large size dusts ( $r_{\text{dust}} \geq 20 \mu\text{m}$  in the first situation and  $\geq 100 \mu\text{m}$  in the second situation) reach to the ergodic layer and heated up to the evaporation/sublimation temperature.

the divertor plates is assumed to be zero. Figures 2 (a) and (b) show the calculated dust trajectories (colored lines) for the first and second situations, respectively (the vacuum vessel is omitted) with indicating the calculated plasma

flow velocity distribution as small colored vectors (some proximate vectors are subtracted). In the first situation, it is assumed that dusts are released with an initial velocity of 5 m/s which is one of the typical ones obtained by an anal-

ysis of three-dimensional dust trajectories using a stereoscopic fast framing camera installed in an outer port. The direction of the velocity is set to that to the plasma center, which means that it assumes the worst condition from a viewpoint of dust penetration into the main plasma. In the second situation, it is supposed that dusts are freely dropped from the upper side in the vacuum vessel. In the both simulation, the initial dust temperature is set to 400 K. The initial specific gravity of the iron and carbon dusts is set to 7.863 and 2.25 g/cm<sup>3</sup>, respectively. The initial specific heat of these two dusts is 0.46 and 0.69 J/gK, respectively.

In the first situation (Fig. 2 (a)), the simulation indicate that small sized iron dusts ( $r_{\text{dust}} \leq 4 \mu\text{m}$ ) are swept off along the plasma flow on a divertor leg which is shown by a red arrow and colored vector plots. It proves that the dominant force affecting on the dust motion is the ion drag force along the plasma flow. The dust trajectories are bent to the upper side by this force because of the high rotational pitch angle ( $\sim 80^\circ$ ) of the magnetic field lines on the divertor leg. For medium sized dusts ( $r_{\text{dust}} = 10 \mu\text{m}$ ), it passes through the divertor leg due to the large momentum effect. The dust trajectory is distorted, then it reaches to the vacuum vessel. For large sized dusts ( $r_{\text{dust}} \geq 20 \mu\text{m}$ ), it reaches to the ergodic layer and evaporates by the heat load due to the higher plasma temperature in the ergodic layer ( $> 50 \text{ eV}$ ). In the largest sized dust case ( $r_{\text{dust}} = 1 \text{ mm}$ ), the simulation predicts that it penetrates into the main plasma (inside of the LCFS), which can enhance impurity radiation in the main plasma.

In the second situation (Fig. 2 (b)), small and medium sized carbon dusts ( $r_{\text{dust}} \leq 40 \mu\text{m}$ ) are dispersed by the plasma flow on the divertor leg to the upper side, which functions to prevent the dusts from reaching to the main plasma. Large sized dusts ( $r_{\text{dust}} \geq 100 \mu\text{m}$ ) penetrate the divertor leg, because the trajectories of the dusts are not significantly distorted in the divertor leg due to the large momentum, and it reaches to the ergodic layer to sublimate there. For the largest sized dust ( $r_{\text{dust}} = 1 \text{ mm}$ ), the simulation shows the penetration of the dust into the main plasma. It suggests that the radii of dusts have to be reduced to less than that in the order of 1 mm in order to protect the main plasma from the dust penetration.

#### 4. Calculations of the Time Evolutions of Dust Parameters

Figure 3 gives the time evolutions of the calculated dust parameters (temperature, mass and velocity) in various sized dust cases for the two situations. The tempera-

ture and velocity of the small/medium sized dusts abruptly increase when it reaches to or passes through the divertor legs at  $t < 10^{-2} \text{ s}$  and  $t \sim 0.2 \text{ s}$  in the two situations, respectively. The temporal change of the two parameters is caused by the effect of the heat load and the ion drag force onto the dusts in the divertor legs, respectively.

The simulation predicts that the velocity of the small sized dusts can be accelerated and reaches to the order of 100 m/s in the divertor legs. Meanwhile, the dust parameters for the large sized dusts are not observably affected by the divertor legs because of the large heat capacity and the large momentum. It also indicates that when the medium and large sized dusts reach to the ergodic layer, the temperature of the dusts abruptly rises and the mass significantly drops because of the high heat loads onto the dusts in the ergodic layer and the main plasma. On the other hand, the temperatures of the small and medium sized dusts do not rise to the evaporation/sublimation temperatures, and the masses are not changed with time. This is because these dusts are not significantly affected by the heat load in the peripheral plasma after leaving from the divertor leg by the effect of the ion drag force due to the plasma flow.

#### 5. Summary

A dust transport simulation code (DUSTT) is implemented in a three-dimensional neutral particle simulation code (EIRENE), which enables to investigate three-dimensional dust trajectories in non-axisymmetric geometries in the LHD. The simulation proves that there are two functions of the LHD peripheral plasma from a viewpoint of protection of the main plasma from dust penetration. One is sweeping of dusts by the plasma flow (mainly due to ion drag force) in the divertor legs, and another one is evaporation/sublimation of dusts by heat load onto the dusts by the high temperature plasma in the ergodic layer.

- [1] K. Saito *et al.*, J. Nucl. Mater. **363-365**, 1323 (2007).
- [2] S. Ohdachi *et al.*, Contrib. Plasma Phys. **50**, 552 (2010).
- [3] J.P. Sharpe *et al.*, J. Nucl. Mater. **313-316**, 455 (2003).
- [4] S. Iwashita *et al.*, Plasma Fusion Res. SERIES **8**, 308 (2009).
- [5] A. Yu. Pigarov *et al.*, J. Nucl. Mater. **363-365**, 216 (2007).
- [6] R.D. Smirnov *et al.*, Plasma Phys. Control. Fusion **49**, 347 (2007).
- [7] Y. Tanaka *et al.*, J. Nucl. Mater. **415**, S1106 (2011).
- [8] T.D. Rognlien *et al.*, J. Nucl. Mater. **196-198**, 347 (1992).
- [9] D. Reiter *et al.*, Fusion Sci. Technol. **47**, 172 (2005).
- [10] M. Kobayashi *et al.*, Fusion Sci. Technol. **58**, 220 (2010).
- [11] K. Koga *et al.*, Plasma Fusion Res. **4**, 034 (2009).